


Alexander Dresel^{1,*}
Ulrich Teipel^{2,3}

Jet Dispersion of Multiwall Carbon Nanotubes and Correlation with Suspension Rheology

A novel jet dispersion technique was developed and investigated which enabled excellent carbon nanotube (CNT) dispersion by high exfoliation at even very low pressure drops. Suitable procedures were developed for the characterization of agglomerate size and fraction of individual CNTs. The appropriate characterization enabled the definition of a dimensionless dispersing parameter and the development of a kinetic model that describes CNT dispersion in dependence of the volumetric energy input. The rheological behavior of CNT suspensions in steady-shear flows was investigated and demonstrated how the agglomerate fracture and CNT individualization influence the suspension viscosity.

 This is an open access article under the terms of the Creative Commons Attribution License, which permits use, distribution and reproduction in any medium, provided the original work is properly cited.

Keywords: Carbon nanotubes, Jet dispersion, Kinetic model, Multiwall carbon nanotubes, Rheology

Received: September 27, 2019; *revised:* March 18, 2020; *accepted:* March 26, 2020

DOI: 10.1002/ceat.201900534

1 Introduction

Carbon nanotubes (CNTs) possess extraordinary particle properties like enormous mechanical strength [1], electrical [2] and thermal conductivity [3] combined with low material densities [4] that assign these particles a high attractiveness for use in the development of innovative materials in a variety of fields. However, the development of CNT applications is challenging since CNTs strongly agglomerate and form bundles, i.e., parallel alignment of individual CNTs, driven by Van-der-Waals attraction and their huge aspect ratios [5,6]. Regarding the Van-der-Waals interactions, a cohesion energy per unit length between two neighboring tubes of -0.1793 eV\AA and -0.4862 eV\AA for CNT diameters of 2.714 \AA ((4,4)-CNT) and 18.997 \AA ((28,28)-CNT) was estimated based on a theoretical approach [7].

The application of CNTs in innovative developments usually demands their dispersion in organic or inorganic fluids which can be achieved by stressing of the agglomerates with mechanical dispersion techniques [8]. Ultrasound dispersion is thereby frequently applied [5,6,8,9] even that it possibly damages and fractures CNTs [5,10] which means that gentle dispersion technologies are necessary for CNT processing. Besides ultrasound processes, CNTs can be basically dispersed in shear fields. Therefore, high shear rates are required that can be achieved by narrow flow geometries and high flow rates as in high-pressure homogenizers [5].

High-pressure dispersion can accomplish a significantly better dispersion compared with ultrasound techniques [11], although the homogenization using high dispersing pressures is reported to possibly fracture CNT lengths [5]. CNT dispersion in milling processes as in stirred media mills can cause

severe damaging, even an increase of CNT amorphism was observed [12]. In addition to the problem of CNT fracture by dispersion, CNTs exhibit poor dispersibility in pure phases and exfoliation can only be achieved in few liquids [13,14].

Regarding the dispersion, an appropriate characterization of the suspensions, particularly of the fraction of individual CNTs and the agglomerate sizes are of main interest. For CNT dispersion, microscopy analyses are basically applied for verifying individual CNTs [15–17]. Spectroscopy techniques like UV-vis [18,19] and fluorescence [20,21] spectroscopy are frequently used for the detection of the CNT dispersion in dependence of dispersion time and concentration. The quantification of the fraction of individual CNTs in the dispersion is difficult since references and standards are not available for CNTs. Amiran et al. [22] and Coleman [6] presented a procedure to estimate CNT exfoliation by determining the CNT concentration with UV-vis-NIR spectroscopy after the separation of remaining agglomerates.

In comparison, the dispersion of nanoparticles is usually characterized by the particle size or size distribution in dependence of dispersing time or specific dispersing energy input [23].

¹Dr.-Ing. Alexander Dresel
Alexander.Dresel@ict.fraunhofer.de
Fraunhofer Institute for Chemical Technology ICT, Joseph-von-Fraunhofer-Strasse 7, 76327 Pfinztal, Germany.

²Prof. Dr.-Ing. Ulrich Teipel
Technical University Nuremberg, Innere Cramer-Klett-Strasse 4–8, 90403 Nuremberg, Germany.

³Prof. Dr.-Ing. Ulrich Teipel
University Ulm, Chemical Engineering, Albert Einstein Allee 11, 89081 Ulm, Germany.

However, particle size analysis cannot detect the CNT length and diameter distributions, and interpretation of detected equivalent diameters is difficult [24,25]. With the size characterization, the kinetics of the dispersion behavior can be expressed. Schilde et al. [26] gave an overview of existing dispersion models and presented a new formulation for modeling of the dispersion of nanoparticles describing the particle size as function of dispersing time or energy. Modeling of the dispersion kinetics enables process optimization by reducing experimental tasks, achieves comparability of different processes, and enhances the understanding of the process and material behavior. Based on the current information of the authors, no dispersion model for CNTs is available.

The rheological behavior of CNT suspensions is substantially influenced by the microstructure of the suspension. The microstructure is thereby defined by the dispersion, aspect ratio, concentration, network structure, and orientation state [27]. Even at low CNT concentrations, undesirable effects as mechanical entanglements and flow-induced clustering appear [28] which can cause significant changes of the rheological behavior [29,30]. In the field of CNTs, process technologies substantially require knowledge about the rheological behavior and suitable techniques like dispersing processes which are able to handle the challenges caused by the rheological properties of such complex systems or allow their adjustment on the suspension rheology.

Here, dispersion and rheology of CNTs are investigated. The studies about the dispersion with a novel jet dispersion technique, the characterization of CNT suspensions, the development of a dispersion model based on a dimensionless dispersing parameter, and the influence of dispersion on the rheological behavior are discussed.

2 Materials and Methods

2.1 Multiwall Carbon Nanotubes (MWNTs) and Particle Size Distribution

MWNTs were employed for the investigation. Particularly, CNT-MW-as synthesized (MWNT^{as}) with a carbon purity of >98% according to the manufacturer (Future Carbon GmbH, Bayreuth, Germany) were used as received without any further modification. Scanning electron images of the as-received MWNT^{as} are presented in Fig. 1. The source material consists of MWNT agglomerates with sizes larger than 100 μm (Fig. 1a) wherein the agglomerates are formed by irregularly arranged individual MWNTs (Fig. 1b) emphasizing the challenge of CNT exfoliation as well as the characterization due to the tubular particle morphology. The MWNT^{as} were dispersed in *N*-methyl-2-pyrrolidone (NMP) which could be shown as appropriate dispersing fluid for CNTs since dispersive and polar components of the surface energies of the particles and the fluid are in good agreement [31].

In order to determine the particle size distribution by differential sedimentation analysis, the particle density and the refractive index of the material are required. The particle density was determined with a gas pycnometer (multivolume pycnometer 1305, Micromeritics) according to DIN 66137

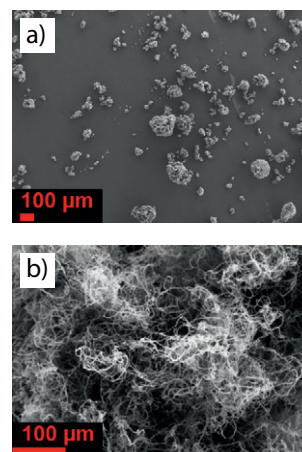


Figure 1. Scanning electron images of the used multiwall carbon nanotubes (MWNT^{as}): (a) overview of MWNT^{as} agglomerates, (b) agglomerate surface formed by individual MWNT^{as}.

[32]. Therefore, the sample was dried at 150 °C for 120 min and analyzed with helium as measuring gas after 20 flushing cycles in the sample cell. The material density was determined with $1.664 \pm 0.0728 \text{ g cm}^{-3}$ (\pm standard deviation) as average from ten single measuring cycles. The refractive index for MWNTs was chosen from literature [25] as estimation for the MWNT^{as} refractive index with a real fraction of ~ 1.11 at a wavelength of 405 nm whereby the imaginary part was not required for the measuring device.

2.2 Jet Dispersion Process

For the CNT dispersion, an innovative jet dispersion technique was developed and realized in a process plant. Jet dispersion is achieved by a specific dispersion nozzle. The nozzle exhibits a radial inlet where the inner diameter decreases to a minimum after which the geometry opens by a sharp increase of the diameter through a conical outlet. An elongational flow of the suspension is achieved through the inlet which is strongly interrupted by the sharp diameter increase in the outlet. Thus, the suspension and the particles are stressed by pressure and velocity gradients that enables the dispersion.

Fig. 2 shows a schematic flow chart of the dispersion process. The suspension is pumped from a tempered vessel (B1) through the dispersion nozzle with an eccentric screw pump (P1) which is also used for pressure adjustment. Afterwards, the suspension is collected in a second tempered container (B2) and a new dispersion cycle can follow. Thus, the process operates alternating which means that the intermixing of the stressed suspension with the non-stressed is minimized in each cycle [33]).

The dispersing behavior of the MWNT^{as} in *N*-methyl-2-pyrrolidone as model system was investigated. The concentration in the suspensions was kept constant with 0.1 wt% and the temperature with 25 °C. In this work, the dispersing pressure difference across the nozzle geometry and the number of dispersing cycles was varied whereby the energy density and the

The measuring assembly basically consists of a light source which leads parallel NIR light through the sample cell on a rotor. The transmission of the dispersion is gathered by a detector. Thus, the intensity of the transmitted light or alternatively light extinction can be detected in dependence of the time and position of the dispersion which allows the characterization of the particle sedimentation during centrifugation.

The analysis was conducted in polyamide cuvettes of a width of 10 mm using a speed ramp from $13 \times g$ to $2325 \times g$ (referred to a radius of 130 mm) at the beginning of the centrifugation followed by the maximum centrifugal acceleration ($2325 \times g$) for a longer period of time. The extinction from the used cuvettes can differ between different sample cells. Since the extinction of the sample cell is low compared with the suspension extinction, these fluctuations may influence measurements in the region of low suspension extinction. Therefore, the extinction of the pure NMP, which served as reference for the analysis, was averaged from ten single measurements.

2.5 Characterization of the Rheological Behavior of MWNT^{as} Suspensions

The rheological behavior was investigated with a rotational rheometer (Universal Dynamic Spectrometer UDS 200, Physica Messtechnik GmbH, Stuttgart, Germany) and a double-gap measuring device (Z1 DIN according to DIN54453 [35]). In particular, the rheological properties of the suspensions were characterized in stationary shear flows. Thereby, the shear rate was varied and the shear stress and the viscosity were determined. For each analysis, the suspension was prestirred and tempered in a water bath prior to its transfer into the measuring cell. The analysis was started after a damping period of 60 s. The temperature was set at 25 °C during the measurements. The resolution of the detected torque shows with 0.01×10^{-6} Nm a very high accuracy of the rheometer. Furthermore, the precision of the measurements was determined by measuring the dynamic viscosity of a standard. The standard material was a calibration oil with a dynamic viscosity in the low viscosity region between 1.6 and 1.1 mPa s at temperatures between 20 °C and 40 °C, respectively. The uncertainty was smaller than 0.3 %.

3 Dispersion of CNTs

3.1 Development of the Particle Size Distribution by Jet Dispersion

The particle size distributions $q_3(\ln x)$ of the suspensions are depicted in Fig. 3a in dependence of the volumetric specific energy input E_V and process cycles n_C of the jet dispersion with a pressure difference of 14.8 bar. The figure shows that the detected particle sizes x in the initial suspension between 1 and 20 μm with a monomodal distribution shift towards smaller sizes by dispersion and thus, increasing specific energy input. The major size decrease is at small energy inputs of up to $1.49 \times 10^7 \text{ J m}^{-3}$ ($n_C = 10$), after which the main particle fraction is smaller than 2 μm and a multimodal size distribution is indi-

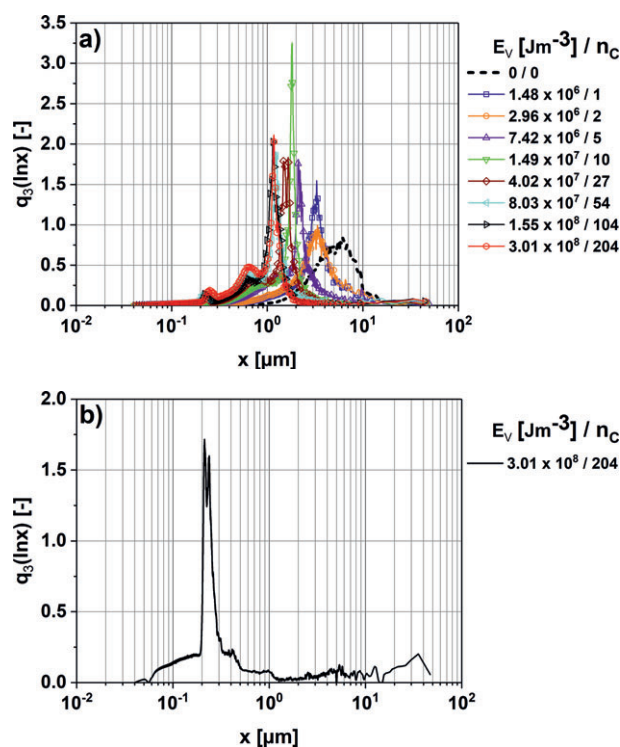


Figure 3. Development of particle size distribution during the jet dispersion of the MWNT^{as} in *N*-methyl-2-pyrrolidone ($w = 0.1 \text{ wt } \%$, $\Delta p = 14.8 \text{ bar}$) in dependence of the volumetric specific energy input (a) and particle size distribution of individual MWNT^{as} (b).

cated with a main particle fraction around 1.9 μm . At very high energy inputs up to $3.01 \times 10^8 \text{ J m}^{-3}$ ($n_C = 204$), the main particle size fraction refers to 1.1 μm and no significant changes of the particle size distributions could be detected with the increasing energy input which depicts the end of the dispersion process with the underlying parameters. This shows clearly dispersion progress and deagglomeration of the CNTs by the jet dispersion process.

Differentiation between agglomerated and individual CNTs within the detected size distributions is difficult, however, can be achieved by consideration of fractionated CNT suspensions [25]. In order to determine the size range of individual CNTs, the agglomerates were removed from the dispersion with a lab centrifuge (Kontifuge 17RS, Heraeus Sepatech, Hanau, Germany) resulting in a dispersion containing a high fraction of individual CNTs. Fig. 3b shows the differential size distribution $q_3^*(\ln x)$ determined with the disc centrifuge of a suspension containing a high fraction of MWNT^{as}. The size distribution shows the majority of the particles between 0.04 and 0.5 μm which can be most probably referred to single CNTs whereas the detected size range $> 1 \mu\text{m}$ is expected to characterize residual agglomerates by the separation method. The size range between 0.5 and 1 μm may indicate CNTs of high lengths since the length varies in a significantly wider range as the diameter whereby the sedimentation velocity, and hence, the Stokes diameter, differ for similar CNT diameters mainly with the CNT lengths.

Nadler et al. [34] determined the region of the Stokes diameter of individual MWNTs at sizes smaller than $0.1 \mu\text{m}$ by differential sedimentation analysis and, hence, postulated a perpendicular orientation of the CNT axis to the direction of sedimentation. The size region of individual CNTs with $< 500 \mu\text{m}$ is significantly greater which is caused by a parallel to the movement oriented CNT. Detailed experimental and theoretical analyses of the particle sedimentation and Stokes diameter are given in [33]. Different orientation is probably caused by the composition of the density gradient, a possible contribution of surfactants, and the properties of the used CNT material.

When the size distribution of individual MWNT^{as} in Fig. 3b is compared with the size distribution of the original suspension, it can be stated that the size region below $0.5 \mu\text{m}$ refers to the equivalent diameter of dispersed individual MWNT^{as} whereas the agglomerates exhibit Stokes diameters greater than $1 \mu\text{m}$. Therefore, the main mode of the size distributions of the suspensions mainly refers to the agglomerates and, thus, can be used as an estimation for the average agglomerate size.

Fig. 4 presents the estimated average agglomerate size based on the Stokes diameter in dependence of the volumetric specific energy input for two dispersion pressures of 9.9 and 14.8 bar. At the beginning of jet dispersion, a sharp size reduction of the agglomerates can be observed after which the sizes only slightly change with higher specific energy inputs. Thereby, the development of the agglomerate fracture is similar for both dispersion pressures and results in an agglomerate size of nearly $1 \mu\text{m}$. This indicates that a similar agglomerate size can be reached for the MWNT^{as} in NMP after jet dispersion with the same volumetric specific energy input.

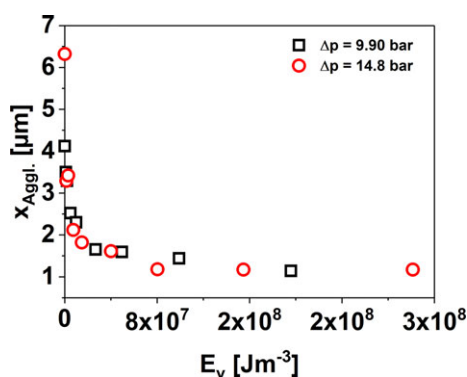


Figure 4. Agglomerate size derived from the density size distribution in dependence of the volumetric specific energy input and dispersing pressure difference.

3.2 Deagglomeration of the MWNTs

Fig. 5 schematically illustrates the time-dependent light extinction of an MWNT^{as} suspension in comparison to the extinction of the pure NMP during centrifugal analysis. The extinction shows a sharp decrease after short sedimentation times caused by particle separation and remains nearly unchanged after long centrifugation as well as a greater extinction compared to the

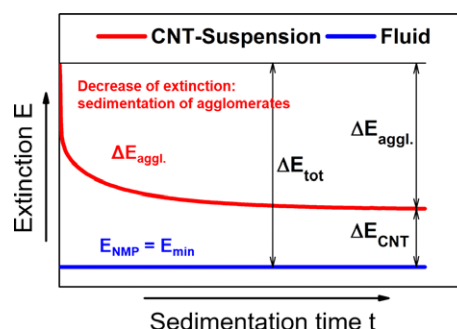


Figure 5. Detection of the particle sedimentation by the time-dependent extinction of the suspension during centrifugation and determination of the degree of deagglomeration.

pure NMP. This means that the extinction decrease is mainly caused by sedimentation of the agglomerates since exfoliated MWNTs sediment significantly slower and cannot be completely separated under these conditions of centrifugal acceleration and time. Therefore, the resulting extinction at longer sedimentation times corresponds to the content of individual CNTs. The procedure of the characterization of the deagglomeration degree used in this work was investigated and developed by the authors and is given in detail in [33].

Since the extinction changes can be applied to differentiate between agglomerated and individual CNTs, the degree of deagglomeration can be derived according to Eq. (3). The remaining extinction difference ΔE_{CNT} of the dispersion to the extinction of the fluid correlates with the exfoliated MWNTs whereby the extinction of the fluid $E_{\text{NMP}} = E_{\text{min}}$ shows the extinction that could be reached if the disperse phase would completely sediment. Furthermore, the difference $\Delta E_{\text{aggl.}}$ between the extinction of the dispersion at the beginning and end of the analysis is caused by the sedimentation of the agglomerates under the assumption that individual nanotubes are not separated. The sum of the extinction differences of agglomerates and individual CNTs refers then to the total possible extinction change of the dispersion ΔE_{tot} .

The change of extinction of the CNTs referred to the maximal possible and observed difference of all respective dispersions $\Delta E_{\text{tot,max}} = \Delta E_{(\text{CNT+aggl.})\text{max}}$ defines the degree of deagglomeration κ_{IE} . A degree of deagglomeration of $\kappa_{\text{IE}} = 0$ characterizes no presence of individual CNTs, a value between 0 and 1 ($0 < \kappa_{\text{IE}} < 1$) is related to the fraction of exfoliated CNTs and $\kappa_{\text{IE}} = 1$ suggests the entire CNT disintegration.

$$\kappa_{\text{IE}} = \frac{\Delta E_{\text{CNT}}}{\Delta E_{(\text{CNT+aggl.})\text{max}}} \quad (3)$$

The degree of deagglomeration is displayed in dependence of the volumetric specific energy input and dispersing pressures in Fig. 6. A tendential increase of the deagglomeration, which means CNT individualization with increasing energy input, can be observed until after higher energy inputs no significant further change could be achieved by the dispersion. This displays the end of the dispersion process with the underlying conditions.

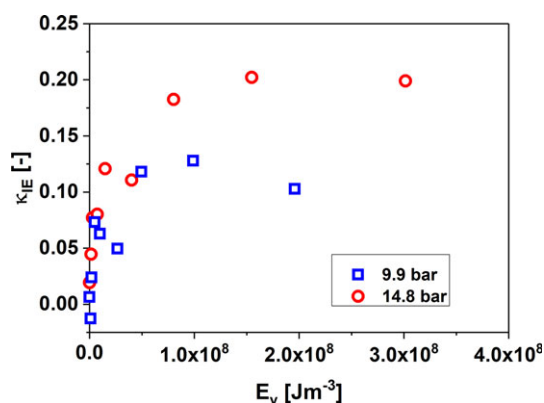


Figure 6. Degree of deagglomeration in dependence of the volumetric specific energy input at different pressure differences.

The strong increase at low energy inputs is caused by the agglomerate size reduction and CNT exfoliation. After longer dispersion, the changes of agglomerate size and individual CNTs decrease which cause a smaller slope of the development of the deagglomeration degree. At lower dispersion pressures, this reduction already occurs at lower energy inputs since the achievable agglomerate fracture and exfoliation caused by the lower mechanical stressing of the particles is less and thus, the end of dispersion previously reached. The decline of the deagglomeration degree at the end of the dispersion with the dispersion pressure of 9.9 bar might be caused by errors during the sampling or the space- and time-resolved sedimentation analyses as, e.g., by particle attachments on the sample cell.

The derived degree of deagglomeration gives an excellent depiction of the deagglomeration progress of individual CNTs from the agglomerates. The dispersion with 14.8 bar achieved a degree of deagglomeration of ~ 0.2 (20 %) whereas the individualization was significantly lower after the dispersion with 9.9 bar.

As opposed to the agglomerate size, the MWNT^{as} deagglomeration scales with the dispersing pressure which is caused by higher pressure and velocity gradients in the nozzle geometry. Though the agglomerate fracture is not significantly altered by the pressure change in the investigated region, the increase of the pressure and velocity gradients enhance the individualization. Particularly, the strain rate, i.e., velocity difference in the inlet of the nozzle referred to the length of the inlet, in the inlet of the nozzle with 3917 s^{-1} at 14.8 bar is significantly higher than 3449 s^{-1} at 9.9 bar pressure difference. Thus, the greater degree of deagglomeration is highly caused by the elongational flow in the nozzle inlet which supports the detachment of individual CNTs from the agglomerates by tensile loading mechanisms.

In order to verify the exfoliation of CNTs, the particles were characterized with transmission electron microscopy (TEM; JEM2100, JEOL Ltd., Tokyo, Japan). In Fig. 7, a TEM image after jet dispersion is presented. Individual MWNT^{as} can be observed which verifies the CNT exfoliation by the new jet dispersion process. Furthermore, the CNTs exhibit a wide variation of the lengths with CNTs longer than $4 \mu\text{m}$. Particularly,

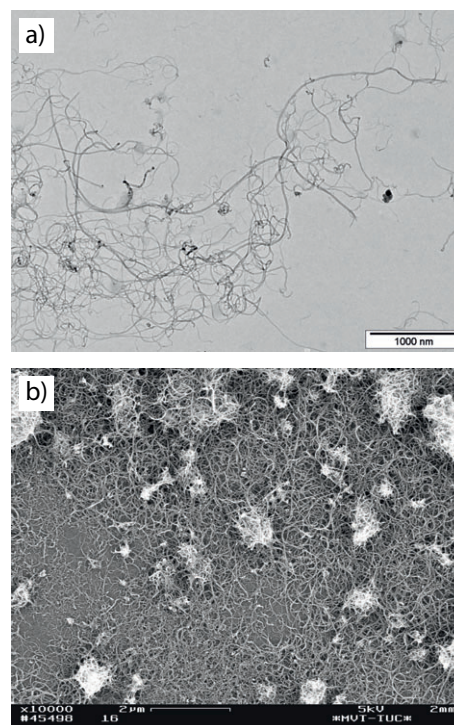


Figure 7. Transmission electron microscopy (a) and scanning electron (b) images of carbon nanotubes after jet dispersion in NMP with a pressure difference of 14.8 bar and volumetric specific energy input of $3.01 \times 10^8 \text{ Jm}^{-3}$.

the very long CNTs which could be separated from the agglomerates indicate a gentle dispersion behavior of the jet dispersion process. Fig. 7b shows an image of the sample from scanning electron microscopy (SEM, Zeiss DSM Gemini 982, Carl Zeiss Microscopy GmbH, Jena, Germany). The image displays the remaining agglomerates after the dispersion that lie on a layer of individual MWNTs. It can be observed that the size of the agglomerates is around $1 \mu\text{m}$ which agrees well with the derived average agglomerate size from the particle size distributions.

3.3 Model for the Dispersion Progress of CNTs

In the suspension, the agglomerate size and the degree of deagglomeration change with the dispersion. Both suspension attributes can be considered with a dimensionless dispersing parameter Ψ (Eq. (4)) which is the product of the degree of deagglomeration and the normalized agglomerate size X . The normalized agglomerate size is given by the quotient of the agglomerate size change, which is the initial agglomerate size at the beginning of the dispersion $x_{\text{aggl},A}$ and the current agglomerate size $x_{\text{aggl},t}$, and the initial agglomerate size. In the case of total exfoliation, agglomerates would not be present in suspension, thus, the agglomerate size $x_{\text{aggl},t}$ would approach 0 and the normalized agglomerate size X would reach 1.

With the degree of deagglomeration derived from the sedimentation analysis, the dispersing parameter can be determined

as in Eq. (5). The parameter refers to the range between 0 and 1 whereby the dispersion increases with higher parameter.

$$\Psi = \kappa\chi \quad \text{with } \chi = \frac{x_{\text{agglo.,A}} - x_{\text{agglo.}}}{x_{\text{agglo.,A}}} \quad (4)$$

$$\Psi = \kappa_{\text{IE}} \frac{x_{\text{agglo.,A}} - x_{\text{agglo.}}}{x_{\text{agglo.,A}}} \quad (5)$$

The dispersing parameter can be expressed by the volumetric specific energy input as in Eq. (6) according to the dispersion model for nanoparticles describing the particle size depending on time or energy [26]. Therein, Ψ_A is the dimensionless dispersing parameter in the initial suspension, Ψ_Ω is the parameter at the end of the dispersion, and Γ denotes the fit parameter which corresponds to that dispersing parameter that is the half increase between the beginning and end of the dispersion.

$$\Psi(E_V) = \Psi_A + (\Psi_\Omega - \Psi_A) \frac{E_V}{E_V + \Gamma} \quad \text{with } \Psi(\Gamma) = \frac{\Psi_A + \Psi_\Omega}{2} \quad (6)$$

Fig. 8 presents the dimensionless dispersing parameter in dependence of the volumetric specific energy input. The parameter becomes greater with increasing energy until the end of the dispersion indicated by the stagnating dispersing parameter at high energy inputs. Thus, the defined parameter describes the dispersion process considering the agglomerate size change and CNT individualization. In comparison to the experimental data, the progression of the dispersing parameter regarding the dispersion model (Eq. (6)) is drawn. The theoretical and experimental progression are in excellent agreement even of scattering experimental data caused by inaccuracies of single sedimentation analyses. This demonstrates that the defined dimensionless dispersing parameter and the derived model can be applied to describe the dispersion of CNTs.

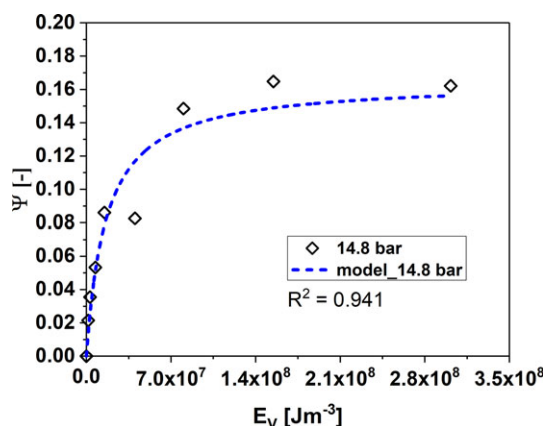


Figure 8. Experimental dispersing parameter in dependence of the volumetric specific energy input at a different pressure difference of 14.8 bar in comparison to the theoretical model.

4 Rheology of MWNT Suspensions in Stationary Shear Flows

The rheological behavior in stationary shear flows is indicated by the dynamic viscosity in dependence of the shear rate in Fig. 9. Particularly, the viscosity functions of suspensions after jet dispersion with different volumetric specific energy inputs are shown in comparison to the viscosity of pure NMP which exhibit Newtonian behavior in the detected region. After dispersion, a significant increase of the viscosity and shear-thinning behavior due to the flow-induced structuring can be observed. At low shear rates, the viscosity first increases with low energy inputs due to agglomerate fragmentation and CNT exfoliation. After dispersion with higher energy inputs of $7.42 \times 10^6 \text{ J m}^{-3}$, the viscosity decreases.

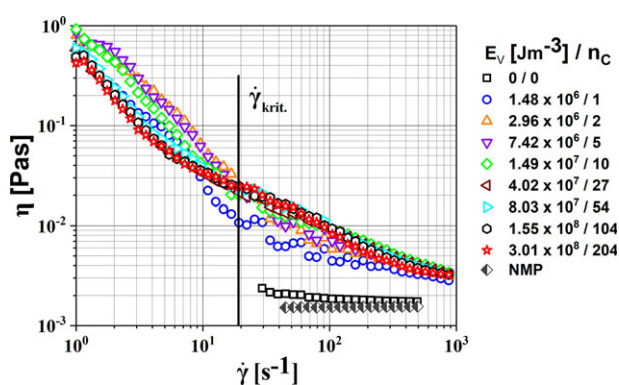


Figure 9. Viscosity in dependence of the shear rate and volumetric specific energy input by the jet dispersion in *N*-methyl-2-pyrrolidone ($w = 0.1 \text{ wt } \%$, $\Delta p = 14.8 \text{ bar}$).

The fluctuating viscosity in the low shear rate region is caused by a flow-induced aggregation [30] of the individual CNTs and CNT agglomerates. In comparison, at high shear rates a tendential rise of the viscosity with increasing energy input of the dispersion can be observed since the flow behavior is based on orientation effects. This viscosity increment results from the agglomerate fragmentation and CNT exfoliation and, thus, characterizes the CNT dispersion process. Furthermore, the flow curves exhibit the same viscosity at $\sim 19.8 \text{ s}^{-1}$ which allows the definition of a critical shear rate that characterizes an equilibrium between hydrodynamic forces and structure-forming interactions. These investigations demonstrate the influence of the agglomerate fragmentation and CNT exfoliation on the rheological behavior. The viscosity in the region of high shear rates can be considered for the correlation of the dispersion with the rheological behavior.

In Fig. 10, the viscosity at a shear rate of 104 s^{-1} is in dependence of the volumetric specific energy input (a) and the development of the dispersing parameter (b). Generally, it can be observed that a dispersing parameter increase correlates with a higher viscosity. Particularly, it demonstrates that the agglomerate fracture and CNT deagglomeration at the beginning of the dispersion lead to a strong increase of the viscosity caused by a structure formation in the suspension between

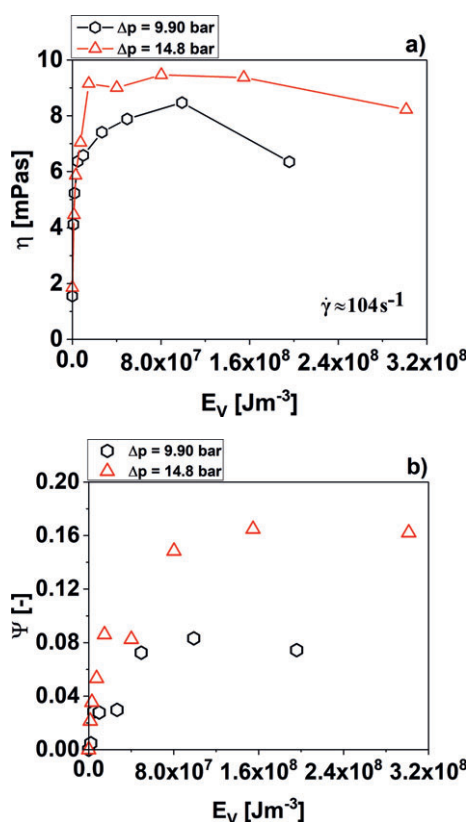


Figure 10. Viscosity at low shear rate (104 s^{-1}) in comparison to the dimensionless dispersing parameter in dependence of the jet dispersion, e.g., volumetric specific energy input and dispersing pressure difference.

agglomerates and individual CNTs which increases the resistance against the flow-induced particle orientation. When comparing the behavior for different dispersion pressure differences, it has to be considered that the progression of the average agglomerate sizes in the suspension is independent of the dispersing pressure (see Fig. 4) whereas the degree of deagglomeration increases with higher pressure (see Fig. 6).

The higher viscosity in the suspension with the increasing dispersing pressure is mainly caused by the greater fraction of individual CNTs leading to a stronger entangled suspension structure between the agglomerates. This indicates that both, agglomerate fracture and CNT deagglomeration, significantly influence the rheological behavior whereby agglomerate size reduction in combination with a small fraction of individual CNTs significantly increase the viscosity by the structure-forming. The individualization contributes also to the suspension structure, however, the influence is lower compared with the agglomerate fragmentation under the investigated conditions.

5 Conclusion

The designed novel jet dispersion process achieved an outstanding CNT deagglomeration demonstrated by a high degree of individual CNTs in the pure liquid phase at even very low

dispersing pressures. High-pressure homogenization usually utilizes significantly higher pressures of up to 350 MPa [36]. In comparison to the jet dispersion of CNTs, ultrasound and rotor-stator dispersion were investigated and operated similarly in a semi-continuous process. Jet dispersion achieved thereby the best CNT dispersion.

Jet dispersion was further investigated in dependence of CNT concentration in the low concentration region between 0.05 and 0.5 wt %. At low CNT concentrations, a lower degree of deagglomeration was observed. For the dispersion in that region of high concentrations, the degree of deagglomeration dropped down after an incipient increase caused by reagglomeration effects.

As discussed, the main parameter of jet dispersion is the strain rate that was further varied by the minimal diameter of the dispersing nozzle. This verified the observation that the dispersing parameter scales with the strain rate. The investigation about the jet dispersion in dependence of concentration and strain rate as well as the comparison to other dispersing technologies are discussed in detail in [33].

By the low dispersing pressure in combination with the smooth flow through the nozzle and the comparison with the other techniques, a gentle dispersion behavior of the jet process for CNTs could be achieved. Particularly, very long exfoliated CNTs shown by TEM analyses verified the gentle dispersion behavior of the jet process for CNTs.

Furthermore, the designed process operates continuously and possesses an enormous potential by the operation parameters and nozzle geometry for further optimization and adaption to other material systems as, e.g., polymers; hence, is highly suited for upscaling and application.

The derived procedures for the characterization of the agglomerate size and the degree of deagglomeration enabled fast methods for differentiating between individual and agglomerated CNTs. Thereby, the characterization is independent from any reference standards that are usually required by spectroscopy methods for determining concentrations. Furthermore, a dimensionless dispersing parameter could be defined which facilitated the development of the introduced dispersion model for CNTs. The model well describes the dispersion progress and allows a better understanding and control. Of main interest is the application of the model as instrument regarding optimization since less experiments have to be performed for estimating the dispersion progress or expected process results.

The dispersion exhibited a significant influence on the suspension rheology whereby shear-thinning behavior and a critical shear rate could be identified even after dispersion with less specific energy input. Under high shearing, particle orientation dominates whereas weak aggregation and once again deagglomeration effects are responsible for an instationary viscosity. In both cases, the flow-induced destructuring is essential for processes and applications dealing with such systems.

The instationarities, aggregation and agglomeration effects and structure-forming are related to the presence of agglomerates and individual CNTs in the suspension. The agglomerate fracture and already small fractions of individual CNTs lead to the formation of an interconnected suspension structure. The structure is significantly influenced by the average agglomerate

size whereby also differences of the degree of deagglomeration affect the network but less strongly than the impact by the agglomerate fracture.

The authors have declared no conflict of interest.

Symbols used

E	[-]	extinction
$\Delta E_{\text{aggl.}}$	[-]	extinction change referred to agglomerates
ΔE_{CNT}	[-]	extinction change referred to CNTs
E_{D}	[J m ⁻³]	energy density
E_{i}	[J]	energy input
E_{min}	[-]	minimal extinction
E_{NMP}	[-]	extinction of <i>N</i> -methyl-2-pyrrolidone
$\Delta E_{\text{tot.}}$	[-]	total extinction change
E_{V}	[J m ⁻³]	volumetric specific energy input
$E_{\text{V,D,i}}$	[J m ⁻³]	volumetric specific energy input per cycle
n_{C}	[-]	number of dispersion cycles
P	[W]	power
Δp	[Pa]	pressure difference
V_{S}	[m ³]	suspension volume
\dot{V}_{S}	[m ³ s ⁻¹]	suspension volume flow rate
$x_{\text{aggl.}}$	[m]	agglomerate size
$x_{\text{aggl.,A}}$	[m]	agglomerate size at the beginning

Greek letters

Γ	[J m ⁻³]	kinetic parameter
X	[-]	normalized agglomerate size change
Ψ	[-]	dimensionless dispersing parameter
Ψ_{A}	[-]	dimensionless dispersing parameter at the beginning
Ψ_{Ω}	[-]	dimensionless dispersing parameter at the end
$\dot{\gamma}$	[s ⁻¹]	shear rate
$\dot{\gamma}_{\text{krit.}}$	[s ⁻¹]	critical shear rate
η	[Pa s]	dynamic viscosity
κ	[-]	degree of deagglomeration
κ_{IE}	[-]	degree of deagglomeration derived from extinction

Abbreviations

CNT	carbon nanotube
MWNT	multiwall carbon nanotube
NMP	<i>N</i> -methyl-2-pyrrolidone
SEM	scanning electron microscopy
TEM	transmission electron microscopy

References

- [1] B. Peng, M. Locascio, P. Zapol, S. Li, S. L. Mielke, G. C. Schatz, H. D. Espinosa, *Nat. Nanotechnol.* **2008**, *3* (10), 626–631. DOI: <https://doi.org/10.1038/nnano.2008.211>
- [2] B. Q. Wei, R. Vajtai, P. M. Ajayan, *Appl. Phys. Lett.* **2001**, *79* (8), 1172. DOI: <https://doi.org/10.1063/1.1396632>
- [3] P. Kim, L. Shi, A. Majumdar, P. McEuen, *Phys. Rev. Lett.* **2001**, *87* (21), 212202-1-215502-4. DOI: <https://doi.org/10.1103/PhysRevLett.87.215502>
- [4] C. Laurent, E. Flahaut, A. Peigney, *Carbon* **2010**, *48* (10), 2994–2996. DOI: <https://doi.org/10.1016/j.carbon.2010.04.010>
- [5] J. Hilding, E. A. Grulke, G. Z. Zhang, F. Lockwood, *J. Dispers. Sci. Technol.* **2003**, *24* (1), 1–41.
- [6] J. N. Coleman, *Adv. Funct. Mater.* **2009**, *19* (23), 3680–3695. DOI: <https://doi.org/10.1002/adfm.200901640>
- [7] L. A. Girifalco, M. Hodak, R. S. Lee, *Phys. Rev. B* **2000**, *62* (19), 13104–13110. DOI: <https://doi.org/10.1103/PhysRevB.62.13104>
- [8] L. Vaisman, H. D. Wagner, G. Marom, *Adv. Colloid Interface Sci.* **2006**, *128–130*, 37–46. DOI: <https://doi.org/10.1016/j.cis.2006.11.007>
- [9] R. Rastogi, R. Kaushal, S. K. Tripathi, A. L. Sharma, I. Kaur, L. M. Bharadwaj, *J. Colloid Interface Sci.* **2008**, *328* (2), 421–428. DOI: <https://doi.org/10.1016/j.jcis.2008.09.015>
- [10] K. L. Lu, R. M. Lago, Y. K. Chen, M. L. H. Green, P. J. F. Harris, S. C. Tsang, *Carbon* **1996**, *34* (6), 814–816.
- [11] S. Azoubel, S. Magdassi, *Carbon* **2010**, *48* (12), 3346–3352. DOI: <https://doi.org/10.1016/j.carbon.2010.05.024>
- [12] N. Darsono, D.-H. Yoon, J. Kim, *Appl. Surf. Sci.* **2008**, *254* (11), 3412–3419. DOI: <https://doi.org/10.1016/j.apsusc.2007.11.028>
- [13] H. T. Ham, Y. S. Choi, I. J. Chung, *J. Colloid Interface Sci.* **2005**, *286* (1), 216–223. DOI: <https://doi.org/10.1016/j.jcis.2005.01.002>
- [14] S. Detriche, G. Zorzini, J.-F. Colomer, A. Fonseca, J. B. Nagy, *J. Nanosci. Nanotechnol.* **2008**, *8* (11), 6082–6092. DOI: <https://doi.org/10.1166/jnn.2008.SW16>
- [15] B. Krause, R. Boldt, P. Pötschke, *Carbon* **2011**, *49* (4), 1243–1247. DOI: <https://doi.org/10.1016/j.carbon.2010.11.042>
- [16] K. D. Ausman, R. Piner, O. Lourie, R. S. Ruoff, M. Korobov, *J. Phys. Chem. B* **2000**, *104* (38), 8911–8915. DOI: <https://doi.org/10.1021/jp002555m>
- [17] M. F. Islam, E. Rojas, D. M. Bergey, A. T. Johnson, A. G. Yodh, *Nano Lett.* **2003**, *3* (2), 269–273. DOI: <https://doi.org/10.1021/nl025924u>
- [18] N. Grossiord, O. Regev, J. Loos, J. Meuldijk, C. E. Koning, *Anal. Chem.* **2005**, *77* (16), 5135–5139. DOI: <https://doi.org/10.1021/ac050358j>
- [19] L. Jiang, L. Gao, J. Sun, *J. Colloid Interface Sci.* **2003**, *260* (1), 89–94. DOI: [https://doi.org/10.1016/S0021-9797\(02\)00176-5](https://doi.org/10.1016/S0021-9797(02)00176-5)
- [20] M. J. O'Connell, P. Boul, L. M. Ericson, C. Huffman, Y. Wang, E. Haroz, C. Kuper, J. Tour, K. D. Ausman, R. E. Smalley, *Chem. Phys. Lett.* **2001**, *342* (3–4), 265–271. DOI: [https://doi.org/10.1016/S0009-2614\(01\)00490-0](https://doi.org/10.1016/S0009-2614(01)00490-0)
- [21] M. S. Strano, V. C. Moore, M. K. Miller, M. J. Allen, E. H. Haroz, C. Kittrell, R. H. Hauge, R. E. Smalley, *J. Nanosci. Nanotechnol.* **2003**, *3* (1/2), 81–86.

- [22] J. Amiran, V. Nicolosi, S. D. Bergin, U. Khan, P. E. Lyons, J. N. Coleman, *J. Phys. Chem. C* **2008**, *112* (10), 3519–3524. DOI: <https://doi.org/10.1021/jp077551x>
- [23] C. Schilde, C. Mages-Sauter, A. Kwade, H. P. Schuchmann, *Powder Technol.* **2011**, *207* (1–3), 353–361. DOI: <https://doi.org/10.1016/j.powtec.2010.11.019>
- [24] B. Krause, M. Mende, P. Pötschke, G. Petzold, *Carbon* **2010**, *48* (10), 2746–2754. DOI: <https://doi.org/10.1016/j.carbon.2010.04.002>
- [25] M. Nadler, T. Mahrholz, U. Riedel, C. Schilde, A. Kwade, *Carbon* **2008**, *46* (11), 1384–1392. DOI: <https://doi.org/10.1016/j.carbon.2008.05.024>
- [26] C. Schilde, I. Kampen, A. Kwade, *Chem. Eng. Sci.* **2010**, *65* (11), 3518–3527. DOI: <https://doi.org/10.1016/j.ces.2010.02.043>
- [27] Z. Fan, S. G. Advani, *J. Rheol.* **2007**, *51* (4), 585. DOI: <https://doi.org/10.1122/1.2736424>
- [28] E. K. Hobbie, D. J. Fry, *J. Chem. Phys.* **2007**, *126* (12), 124907. DOI: <https://doi.org/10.1063/1.2711176>
- [29] S. Lin-Gibson, J. A. Pathak, E. A. Grulke, H. Wang, E. K. Hobbie, *Phys. Rev. Lett.* **2004**, *92* (4), 48302. DOI: <https://doi.org/10.1103/PhysRevLett.92.048302>
- [30] A. W. K. Ma, M. R. Mackley, S. S. Rahatekar, *Rheol. Acta* **2007**, *46* (7), 979–987. DOI: <https://doi.org/10.1007/s00397-007-0183-x>
- [31] A. Dresel, U. Teipel, *Colloids Surf. A* **2016**, *489*, 57–66. DOI: <https://doi.org/10.1016/j.colsurfa.2015.10.027>
- [32] DIN Deutsches Institut für Normung e. V., *Bestimmung der Dichte fester Stoffe - Teil 2: Gaspyknometrie (DIN 66137-2)*, Beuth Verlag, Berlin **2004**.
- [33] A. Dresel, *Dissertation*, Technische Universität Clausthal **2018**.
- [34] S. Tesch, B. Freudig, H. Schubert, *Chem. Ing. Tech.* **2002**, *74* (6), 875–880. DOI: [https://doi.org/10.1002/1522-2640\(200206\)74:6<875:AID-CITE875>3.0.CO;2-8](https://doi.org/10.1002/1522-2640(200206)74:6<875:AID-CITE875>3.0.CO;2-8)
- [35] DIN Deutsches Institut für Normung e. V., *Prüfung von Materialklebstoffen und Metallklebungen; Bestimmung der dynamischen Viskosität von anaeroben Klebstoffen mittels Rotationsviskosimetern (DIN54453)*, Beuth Verlag, Berlin **1982**.
- [36] M. Pohl, H. P. Schuchmann, H. Schubert, *Chem. Ing. Tech.* **2005**, *77* (3), 258–262. DOI: <https://doi.org/10.1002/cite.200407020>